**IMPROVED CRATER WALL SLOPE DETECTION USING A HOUGH CIRCLE TRANSFORM WITH APPLICATIONS TO MARS CRATER MORPHOMETRY AND CLIMATE HISTORY.** B. D. Boatwright[1], J. W. Head[1], and M. A. Kreslavsky[2], [1]Dept. of Earth, Environmental, and Planetary Sciences, Brown University, Providence, RI 02912 USA, [2]Dept. of Earth and Planetary Sciences, University of California Santa Cruz, Santa Cruz, CA 95064 USA (benjamin_boatwright@brown.edu).

**Introduction:** Crater wall slopes are an important morphometric parameter for characterizing diffusive crater degradation processes on the terrestrial planetary bodies [1-8]. Diffusive degradation is believed to be responsible for the shallowing of crater wall slopes over time; thus, the extent of wall slope shallowing may be used as a proxy for the amount of diffusive degradation a crater has undergone, given that the degradation rate is known [6-8]. However, the exact mechanism of diffusive crater degradation on Mars is not known with certainty. Unlike on the Moon, impact cratering has not been widely considered in the context of diffusive degradation on Mars, even though it has inevitably played a role in shaping the surface throughout its history [9].

Using a numerical diffusion model, we presented evidence that impact bombardment on Mars could have made a significant contribution to diffusive crater degradation, even in a 1-bar atmosphere [10]. In order to quantify the extent of this degradation in our model, an efficient measurement technique to obtain crater wall slopes from both measured topographic data as well as model results was necessary. We reported the results of a wall slope detection algorithm for craters with simple bowl-shaped morphologies ($D$ = 1-7 km) in Tyrrhena Terra [11] that closely followed the methodology of a previous survey of crater wall slopes on Mars [12]. Here, we detail significant improvements that have been made to the algorithm, present revised estimates for crater wall slopes in the Tyrrhena Terra study area, and outline new methods that we have used to determine diffusivity values for future modeling of diffusive crater degradation on Mars.

**Improved wall slope detection algorithm:** The primary function of the algorithm is to automate the process of generating radial topographic profiles of crater walls to measure their wall slope. This process involves 1) detecting where a crater is located within a DEM; 2) obtaining radial topographic profiles; and 3) determining the positions along the profile of the rim and floor to accurately measure the rim-to-floor wall slope. We use 75 m/pix HRSC DEMs because they represent a suitable compromise between resolution and spatial coverage.

Step 1 is necessary because of the occasional misregistration between the location of a crater in the database [13] and in the DEM. Previously, the algorithm relied on detecting topographic minima within crater floors to find a center point; however, this quickly ran afoul of problems in cases where the crater center was not also the minimum elevation point. Seeking out a more robust method of center point detection, we turned to a circle-finding algorithm known as the Hough circle transform [e.g. 14]. The Hough transform calculates the likelihood that each pixel within an image is the center of a circle based upon the similarity in pixel values within a given radius range of that point. In our case, the algorithm was detecting points of similar elevation corresponding to crater rim crests. We found the algorithm was largely robust against uneven rim crest topography as well as craters overprinted on steep regional slopes. In addition to the Hough transform, we employed a weighting function such that the likelihood of a detected circle being chosen decreased exponentially away from the mapped crater center in the database. The Hough transform successfully detected crater centers in 246 out of 269 cases (91%), which we confirmed via manual inspection of the DEMs. The remaining 9% were errors due to failure of the transform to detect the correct crater center, usually because the crater misregistration was too extreme to be compensated by the weighting function.

Steps 2 and 3 are relatively more straightforward. Radial topographic profiles were taken in the four cardinal directions up to 1.25x the crater radius to account for possible database measurement errors. The point of maximum topographic curvature closest to the crater center was taken as the floor point (base of the crater wall), and the next closest point of minimum topographic curvature was taken as the rim crest. We used the same rim crest and floor points to compute average rim-to-floor wall slopes for each crater regardless of the location of the steepest segment, which typically changes as the crater degrades. The maximum value among the four average wall slopes was chosen as the representative wall slope for the entire crater. We used the maximum because many craters are partly degraded or buried and thus may not represent the true slope of an otherwise unaltered crater wall.

**Revised estimates of Tyrrhena Terra wall slopes:** Using the improved wall slope detection algorithm, we revisited the crater wall slope measurements we reported previously for the Tyrrhena Terra study area. This area was chosen due to its combination of high crater density and minimal fluvial dissection and dust cover. Details of our DEM processing pipeline are given in previous work [11].

We measured wall slopes for 246 craters with simple morphologies ranging in diameter from 1-7 km (Fig. 1). Fassett & Thomson [4] and others have demonstrated that complex craters with terraced walls on the Moon do

not fit a linear diffusive profile, suggesting that there may be a significant nonlinear component in the degradation of larger craters; we assume that a similar phenomenon may be true for Mars and omit craters with $D$ > 7 km (the simple-to-complex transition diameter) from our study. The median wall slope for the entire population was 13.1˚, slightly higher than our previously reported value of 12˚. Similarly, median slopes were 11.3˚ vs. 10˚ and 26.6˚ vs. 23˚ for craters $D \leq 2$ km and $D > 2$ km, respectively. The slight overall increase in reported median slope is likely a direct result of the improved algorithm, which significantly decreases the number of off-center detections that would result in oblique profiles and thus lower reported slopes.

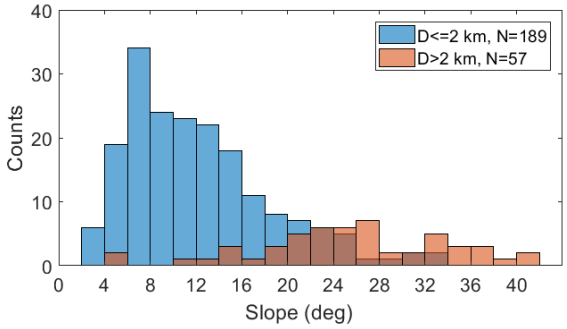


**Fig. 1.** Distributions of crater wall slopes for simple craters observed in the database.

**Future modeling of diffusive crater degradation:** This study is part of an ongoing project to characterize the degradation of small craters on Mars in order to assess the potential significance of impact bombardment in comparison to climate-dependent processes [7,15]. In order to do so, we have expanded upon our previous methods for determining impact-induced diffusivity on Mars.

Our model uses an implicit Euler method to solve the 2-D diffusion equation for the evolution of surface elevation $z(x,y)$ through time $t$:

$$\frac{\partial z}{\partial t} = k\left(\frac{\partial^2 z}{\partial x^2} + \frac{\partial^2 z}{\partial y^2}\right) \quad (1)$$

The diffusivity $k$ (m$^2$/yr) is controlled by the degradational mechanisms inherent to the process being modeled. On the Moon, diffusive crater degradation occurs primarily through impact bombardment [1-3]. Diffusivity for the Moon has been obtained as a function of time from ~3.5 Ga [4,16], and observational evidence suggests that effective diffusivity depends on the starting crater diameter $D$ (i.e. anomalous diffusion) [16].

We extrapolate the lunar diffusivity to Mars in order to assess the contribution of impact bombardment to crater degradation. This extrapolation accounts for two factors. First, impact-induced diffusivity is proportional to the crater formation rate. For small craters, the Mars/Moon cratering rate is ~0.5 [17], and its dependence on crater size is negligible. Second, atmospheric filtering eliminates the contribution of the smallest projectiles whose diameters are smaller than $L$ [18] that would produce craters smaller than $D_{min}$ [19]:

$$L = 0.15P/(\rho g \sin\theta) \quad (2)$$

$$D_{min} = 1.16L^{0.78}(v \sin\theta)^{0.43} g^{-0.22} \quad (3)$$

Here $\rho$ = 3000 kg/m$^3$ is the average impactor density, $g$ = 3.71 m/s$^2$ is the gravitational acceleration, $v$ = 9.6 km/s is the average impact velocity, and $\theta$ = 45˚ is the average impact angle. $P$ is the atmospheric pressure, which we vary over a simple exponential decay from 1 bar at 4 Ga to the modern of value of 0.006 bar [20].

We estimate the missing diffusivity contribution $\Delta k$ of craters smaller than $D_{min}$ using a theoretical treatment of impact-induced diffusion [21] with a power law crater production function $N(>D) \propto D^{-\eta}$. Using the recommended parameter values from Eqs. 27-28 of Minton et al. [21], we derive:

$$\frac{\Delta k}{k} = 1.6^{2-\eta/2}\left(\frac{\eta}{2} - 1\right)\left(\frac{D_{min}}{D}\right)^{4-\eta} \quad (4)$$

For $P$ = 1 bar, $D$ = 1 km, and $\eta$ = 3.2 [18], these equations give $D_{min}$ ~ 68 m and $\Delta k/k$ ~ 8%. For lower $P$ and larger $D$, $\Delta k/k$ is even lower. Thus, atmospheric filtering reduces diffusivity by less than 10% even in a 1-bar atmosphere. These estimates show that atmospheric filtering would have had relatively little effect on impact-induced diffusive degradation for craters larger than 1 km on Mars.

In combination with other ongoing work [22], these simulations will test to what extent a warm and wet early Mars climate is necessary to explain morphometric observations of ancient surface features.

**References:** [1] Head J.W. (1975) The Moon 12, 299-329; [2] Soderblom L.A. (1970) JGR 75, 2655-2661; [3] Craddock R.A., Howard A.D. (2000) JGR 105, 20387-20401; [4] Fassett C.I., Thomson B.J. (2014) JGR 119, 2255-2271; [5] Minton D.A. et al. (2019) Icarus 326, 63-87; [6] Craddock R.A. et al. (1997) JGR 102, 13321-13340; [7] Craddock R.A., Howard A.D. (2002) JGR 107(E11), 5111; [8] Forsberg-Taylor N.K. et al. (2004) JGR 109, E05002; [9] Carr M.H., Head J.W. (2010) EPSL 294, 185-203; [10] Boatwright B.D., Head J.W. (2019) LPSC 50, #2612; [11] Boatwright B.D. et al. (2020) LPSC 51, #2376; [12] Kreslavsky M.A., Head J.W. (2018) GRL 45, 1751-1758; [13] Robbins S.J., Hynek B.M. (2012) JGR 117, E05004; [14] MATLAB Documentation, https://www.mathworks.com/help/images/ref/imfindcircles.html; [15] Ramirez R.M., Craddock R.A. (2018) Nature Geos. 11, 230-237; [16] Fassett C.I. et al. (2018) LPSC 49, #2083; [17] Ivanov B.A. (2001) Chron. Evol. Mars 96, 87-104; [18] Melosh H.J. (1989) Oxford U. Press; [19] Schmidt R.M., Housen K.R. (1987) Intl. J. Impact Eng. 5, 543-560; [20] Warren A.O. et al. (2019) JGR 124, 2793-2818; [21] Minton D.A. et al. (2019) Icarus 326, 63-87; [22] Boatwright B.D., Head J.W. (2021) PSJ, in press.